Dementia Severity Index: A Threshold-Based Approach to Classifying Dementia Level

Shivani Ranjan
Indian Institute of Technology Delhi
Lalan Kumar
lkumar@ee.iitd.ac.in

Indian Institute of Technology Delhi

Research Article

Keywords:

Posted Date: March 18th, 2024

DOI: https://doi.org/10.21203/rs.3.rs-4092892/v1

Additional Declarations: No competing interests reported.

Dementia Severity Index: A Threshold-Based Approach to Classifying Dementia Level

Shivani Ranjan[1] and Lalan Kumar[2*]

***Abstract*— Dementia is marked by a progressive decline in cognitive and emotional capacities, presenting significant challenges to daily functioning. This includes prominent neurodegenerative disorders like Alzheimer's disease (AD) and Frontotemporal dementia (FTD). Recent advancements in electroencephalogram (EEG) sensors and processing tools, project it as a potential biomarker for detecting neuronal and cognitive changes associated with various dementia types. Investigations related to characterization and differentiation are yet to be explored for range identification and assigning quantitative values to resting state EEG from different dementia conditions. In this study, two features that capture the band-specific alterations are computed for each subject. These attributes formed the basis of the Dementia Severity Index (DSI), a threshold-based methodology designed to categorize individuals into AD, FTD, and HC from resting EEG. The introduced thresholding technique underwent validation using machine learning methodologies, specifically the k-nearest neighbors algorithm (kNN) and random forest (RF), achieving accuracies of 81.6$\%$ and 81.37$\%$, respectively. The classification outcomes of derived DSI from F_1 and F_2 are compared. The DSI corresponding to significant feature F_1 is validated on two diverse EEG datasets. The study aims to contribute to the field by providing a set of dementia indexes capable of distinguishing between AD and FTD-based dementia and discriminating against HC. Additionally, the ability of significant features to reflect cognitive performance is explored using the Spearman correlation coefficient (r) to quantify the relationship between predicted Mini-Mental State Examination (MMSE) and actual MMSE scores. The study also delves into the variations in sensor and source domain classification using features F_1 and F_2. The findings of the proposed approach hold promise for capturing a range of values that can effectively classify AD, FTD, and HC, while also offering the advantage of computationally efficient classification when compared with the existing subjective assessment.**

I. INTRODUCTION

Dementia is characterized by a progressive decline in cognitive function that hinders daily functioning and impacts movement, desire, and reaction time [1]. It is a neurodegenerative disorder leading to the degeneration of nerve cells in the brain, causing impaired intercellular communication [2], [3]. The anticipated number of diagnosed dementia cases is poised to double every 20 years, potentially reaching 65.7 million by 2030 [4]. The likelihood of experiencing dementia rises with age, starting at around 1$\%$ between ages 60 and 64 and escalating to 24–33$\%$ for individuals aged 85 and above [5]. Early-onset dementia, appearing before 65, and late-onset dementia, appearing after this age, present distinct challenges. Dementia, stemming from various causes, may also be reversible if diagnosed timely [6].

The primary causes of early-onset dementia are Alzheimer's disease (AD) and Frontotemporal dementia (FTD). AD predominantly affects the hippocampus and memory-associated areas [7], while FTD primarily impacts the frontal and temporal lobes, influencing behavior and language [8]. Distinguishing between F and A based on factors such as diminished focus, executive function, or decreased memory has often yielded uncertain or conflicting outcomes [9]. Given the frequent misdiagnosis of AD and FTD, there is a critical need to develop a more accurate method of differentiating these conditions.

A variety of screening tools, such as the Clinical Dementia Rating (CDR) [10], Mini-Mental State Exam (MMSE) [11], Montreal Cognitive Assessment (MoCA) [12], and Addenbrooke's Cognitive Examination III (ACE-III) [13], are widely employed for the detection of cognitive impairment. Among these tools, the Clinical Dementia Rating (CDR) stands out as the most well-known and extensively researched dementia staging instrument [14]. Moreover, Addenbrooke's Cognitive Examination III (ACE-III) plays a crucial role in dementia diagnosis, particularly in distinguishing between Alzheimer's and frontotemporal dementia [13]. The MMSE, owing to its practical utility and widespread availability, is predominantly utilized for the detection of cognitive impairment [15]. These screening tools assess questionnaire performance, specifically designed to capture functional measures. However, it's important to note that these screening tools exhibit lower sensitivity to the effects of education and premorbid intelligence. These assessments involve an extensive rater certification process and require approximately 30 minutes for administration. Additionally, they demand clinical judgment during both the administration and scoring processes [14], [13].

Functional assessment is essential for distinguishing normal aging from mild cognitive impairment (MCI) and MCI from AD. Additionally, they aid in tracking A progression and differentiating AD from other dementia cases. Neuroimaging techniques, such as magnetic resonance imaging (MRI) [16], [17], [18] and single-photon emission tomography (SPET) [19], have significantly contributed to diagnosing AD and FTD [9]. One takes such functional and behavioral assessment after displaying considerable neurodegeneration and it may lead to irreversible condition. Consequently, forecasting the onset of AD or FTD holds crucial implications.

A timely diagnosis is imperative, as treatment can enhance

[1] Shivani Ranjan is with the Electrical Engineering Department, IIT Delhi, New Delhi, India. eez208482@iitd.ac.in

[2*]Lalan Kumar is with the Electrical Engineering Department, Yardi School of Artificial Intelligence and Bharti School of Telecommunication, IIT Delhi, New Delhi, India. *Correspondence:lkumar@iitd.ac.in

the quality of life by delaying the onset of worsening symptoms [20]. Early detection is challenging but helps in safety measures, planning for money and legal matters, and providing emotional support. This assists patients and families in dealing with the challenges. Therefore, there is a need for innovative detection techniques that can timely identify AD and FTD cases, and ultimately improve the prognosis for affected individuals.

The electroencephalogram (EEG) has garnered significant attention in both research and clinical practice over the past two decades due to its potential as a non-invasive instrument with sensitivity for diagnosing dementia and classifying its severity [21]. An EEG-based approach is preferred for dementia diagnosis and classification due to its non-invasiveness, cost-effectiveness, widespread availability, and faster processing speed compared to other neuroimaging devices [21].

Previous studies have delved into the differences in quantitative EEG among patients with FTD and AD. Spectral analysis of delta and theta frequencies, coupled with episodic memory, has emerged as a robust predictor of FTD and AD. Notably, AD patients exhibit higher diffuse delta/theta activity and lower central/posterior fast frequency bands than H [22], [23]. Furthermore, FTD and AD patients demonstrate diffusely higher theta power in the power spectrum, along with decreased alpha2 and beta1 values in the central and temporal regions [24]. Another study observed lower alpha1 activity in the orbital frontal and temporal lobes of FTD patients, accompanied by higher delta and lower beta1 activity in the frontal and parietal lobes, respectively, when compared to HC [25]. However, the existing research has primarily concentrated on the spectral and quantitative information of EEG signals obtained from scalp electrodes. Limited studies have explored the dynamics to achieve a quantitative value for assessing cognitive decline in FTD, AD, and HC from scalp EEG. Investigations related to characterization and differentiation are yet to be explored for range identification leading to assigning a quantitative value to different dementia conditions during rest.

The objective of the present study is to introduce a thresholding-based approach using the Dementia Severity Index (DSI) to assess dementia levels and classify AD, FTD, and HC cases. Employing EEG source imaging and spectral analysis of spatially distributed information, the study aims to establish a quantitative threshold that can distinguish between different types of dementia and H. Machine learning algorithms such as Random Forest (RF) and K-nearest neighbor (kNN) are utilized to validate the DSI based classification. The study leverages resting-state EEG, which is particularly advantageous for patients as it requires minimal cooperation and causes negligible stress. Additionally, to validate the robustness of the threshold-based DSI approach, the proposed method is applied to two online EEG datasets: the first containing all three cases (AD, FTD, and HC), while the second contains only AD and HC cases. The proposed method exhibits significant potential for real-time applications in identifying FTD and AD in healthy individuals, offering reduced computational processing and a low-cost solution.

II. Methods and Materials

The schematic methodology description to investigate the classification of AD, FTD, and HC based on dementia severity index (DSI) using features (F_1, F_2) is elucidated in Figure 1.

A. Data

The data for this study was collected from 88 subjects at the Department of Neurology of AHEPA General University Hospital in Thessaloniki, Greece. The subjects were divided into three groups: 36 with Alzheimer's disease (AD), 23 with Frontotemporal dementia (FTD), and 29 Healthy Controls (HC) [26]. The Mini-Mental State Examination (MMSE) was used to assess cognitive and neuropsychological function. The MMSE score ranges from 0 to 30, with lower scores indicating greater cognitive decline. The mean (SD) MMSE scores for the AD, FTD, and HC groups were 17.75 (4.5), 22.17 (8.22), and 30 (0), respectively. The mean (SD) ages of the AD, FTD, and HC groups were 66.4 (7.9), 63.6 (8.2), and 67.9 (5.4) years, respectively. The disease duration was assessed in months, with a median value of 25 and an interquartile range (IQR) of 24 to 28.5 months. No comorbidities were reported for the AD group.

B. EEG Recording

Publicly available EEG data from the 88 participants [26] is utilized in this study. The data was recorded using Nihon Kohden EEG 2100 clinical device. In accordance with the 10-20 international system, 19 scalp electrodes were positioned accompanied by two reference electrodes (A1 and A2) on the mastoids for impedance monitoring. Prior to each recording, skin impedance was confirmed to be below 5 $k\Omega$. The EEG data was sampled at a rate of 500 Hz with a resolution of 10 uV/mm. Both anterior-posterior bipolar and referential montages were employed, with Cz serving as the common reference.

C. Pre-processing

The EEG data underwent rigorous preprocessing using MATLAB [27] and the EEGLAB plugin [28]. Initial steps involved band-pass filtering (0.5-45 Hz) employing a Butterworth filter and re-referencing to A1-A2 [26]. To remove non-cerebral artifacts, the Artifact Subspace Reconstruction Routine (ASR) [29] was applied. This technique surpassed conventional artifact rejection thresholds (0.5-second window, 17 standard deviations) by identifying and eliminating bad data periods that significantly improves the data quality. Subsequently, Independent Component Analysis (ICA) was employed to decompose the EEG data into independent source activities [30]. Several ICA components may represent muscle and eye movement artifacts. The EEGLAB "ICLabel" tool was utilized to automatically identify and exclude such artifact-related components classified as "eye artifacts" or "jaw artifacts." This ensured the retention of neural components that enhanced the signal-to-noise ratio.

TABLE I: Table represents the demographic information of the data

Group	N	MMSE_mean	MMSE_std.dev	Age_mean	Age_std.dev	Disease_duration_median	Disease_duration_IQR
AD	36	17.75	4.5	66.4	7.9	25	24
FTD	23	22.17	8.22	63.6	8.2	25	24
HC	29	30	0	67.9	5.4	25	24

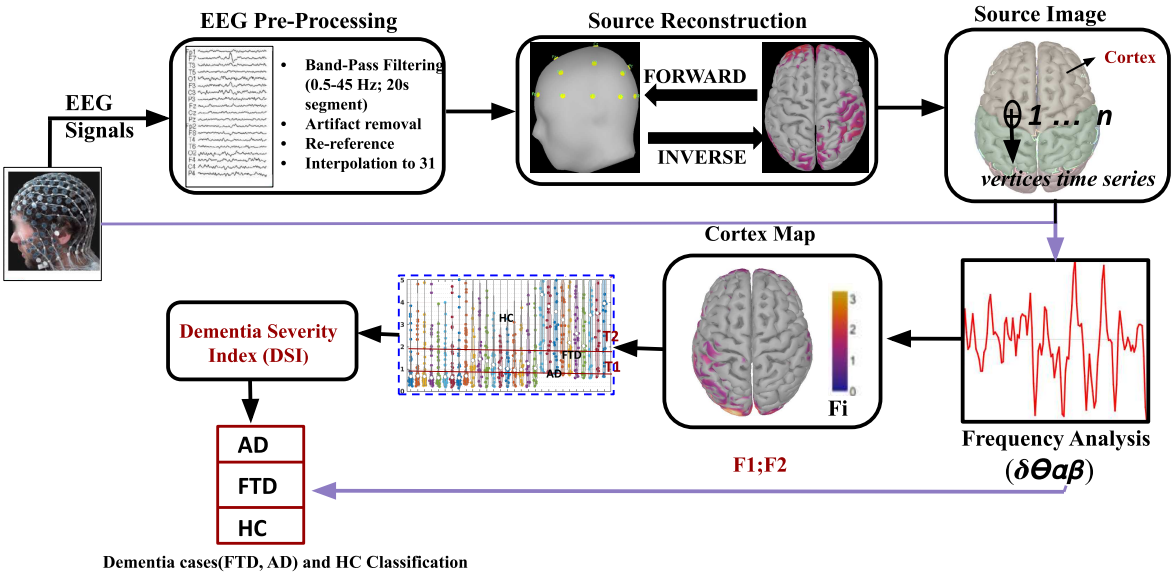

Fig. 1: Schematic flow diagram utilized to investigate the classification of AD, FTD, and HC based on DSI using features (F_1, F_2).

D. Sensor to source mapping

EEG source localization seeks to identify the primary cortical current sources generating the measured scalp potentials [31], [32]. This approach overcomes the limitations of electrode cross-correlation due to volume conduction effects [32]. The localization pipeline comprises of forward and inverse problem solving.

1) Potential, Current Relationship - The Forward Problem: The forward problem establishes the relationship between cortical currents and scalp potentials using a lead field matrix [33]. This matrix simulates the propagation of currents through various head tissues (scalp, skull, brain) using Neumann and Dirichlet boundary conditions [34]. Mathematically, this relationship is expressed as

$$V = A\tilde{S} + Z \tag{1}$$

where V is EEG scalp potential, A is lead field matrix, $\tilde{S}$ is cortical source current, and $[Z]$ is sensor noise matrix. The lead field matrix was computed using the Numerical Boundary Element Method (BEM) [35]. Brainstorm toolbox [36] was utilized for this purpose. The selection facilitated efficient and accurate modeling of the influence of head tissues on current propagation. The preprocessed EEG data from 19 channels was spatially interpolated to 31 channels to augment sensor density and enhance source localization precision [37], [38], [39]. The default cortex model, featuring 15002 vertices, was employed for source estimation. It is noteworthy that the typical number of considered EEG channels is still around 30, while the estimated number of current dipoles is approximately 15,000.

2) sLORETA - The Inverse Problem: The inverse problem in EEG source localization builds upon the established lead field matrix (A) from the forward problem. Its objective is to estimate the hidden cortical source (or vertices) current signal ($\tilde{S}$) that best explains the recorded scalp potentials. To account for potential inaccuracies in the estimated source currents, a noise perturbation matrix (Z) is incorporated into the model. In this study, the standard low-resolution electrical tomography (sLORETA) [40] method is employed as the inverse solution method. sLORETA leverages the principle of spatial smoothness, assuming that neighboring brain regions are more likely to be engaged in the same neural process [41]. This assumption finds further support in the known anatomical and functional connectivity within the brain. By enforcing spatial coherence and consistency in the estimated electrical activity across adjacent voxels, sLORETA seeks to enhance the accuracy and localization precision of the source maps [42]. The source (or vertices) matrix $\tilde{S}$ is estimated by solving the following optimization problem:

$$\min_{S} F = ||V - AS||_2 + \lambda||S|| \tag{2}$$

The solution to the optimization problem using sLORETA is given as [42]

$$\tilde{S} = A^T \left[AA^T + \lambda H\right]^+ V = A_{sLORETA} V \qquad (3)$$

where H is the average reference operator and and $A_{sLORETA}$ is the inverse Kernel that relates the recorded scalp potential V to the cortical source current (or vertices) estimate $\tilde{S}$.

For a more in-depth examination of the cortical source (or vertices) currents defined by the matrix $\tilde{S}$ obtained through source localization, the entire brain underwent parcellation into distinct regions of interest. This study utilized the Desikan Killiany Atlas [43] for a detailed analysis featuring 68 regions. Within each region, the respective cortical source current signals were averaged, yielding a set of time series that represent the average activity in each brain region. This process resulted in scout time series matrices $\tilde{S}_R$ that capture the brain region data. These matrices (V, $\tilde{S}$, and $\tilde{S}_R$) provide the foundation for subsequent feature extraction and, ultimately, the computation of the DSI.

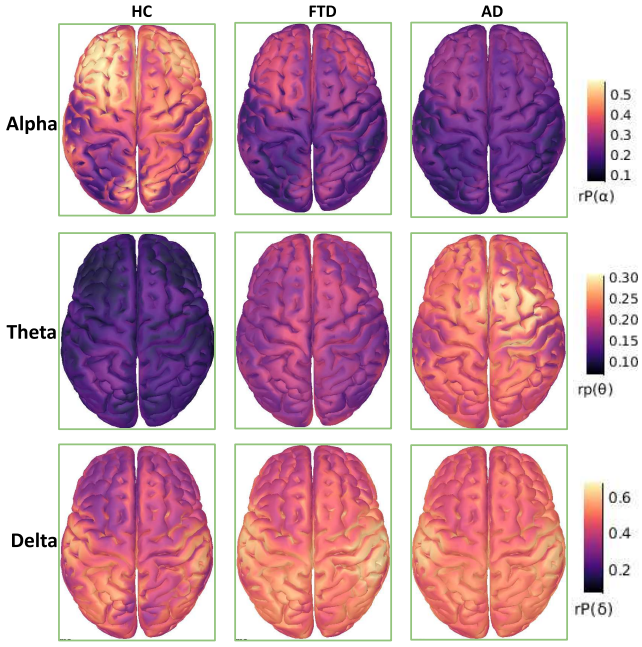

Fig. 2: Cortex map representation of rP (α, θ, δ) alterations observed in AD, FTD and HC. The image is generated using Brainstorm Toolbox

E. Feature Extraction

In this Section, the computation of DSI from Power Spectral Density (PSD) is detailed.

1) Power Spectral Density: The estimated cortical source signals ($\tilde{S}$, $\tilde{S}_R$) and processed scalp potential (V) are utilized for spectral analysis using power spectral density to scrutinize the distribution of power across various frequency bands. In particular, delta (δ: 0.5–4 Hz), theta (θ: 4–8 Hz), and alpha (α: 8–12 Hz) bands known for their association with altered functioning in dementia, are studied [44]. These bands are correlated with distinct cognitive and neurological processes, encompassing slow-wave sleep (delta), attention and memory (theta), and neuronal synchronization and inhibition (alpha) [45].

The power spectral density for the measured or estimated parameters ($V, \tilde{S}, \tilde{S}_R$) is computed using the Welch method implemented in the Brainstorm toolbox [46], [36]. This method is selected for its capability to handle non-stationary signals. Following the PSD computation, relative power ratio (rP) for frequency band B is proposed to be computed as

$$rP_B = \frac{\int_{f\in B} P(f)df}{\int_{f_{min}}^{f_{max}} P(f)df} \qquad (4)$$

where, $P(f)$ denotes PSD function, $\int_{f\in B} P(f)df$ indicates power over frequency band B, and $\int_{f_{min}}^{f_{max}} P(f)df$ is the power over the entire frequency range of interest ($\delta : 0.5 - 4Hz, \theta : 4 - 8Hz, \alpha : 8 - 12Hz, \beta : 12 - 29Hz, \gamma : 30 - 45Hz$)

The relative power quantifies the power distribution across different frequency bands, reflecting the contribution of specific brain rhythms to the overall activity. Thus the ratio offers a normalized assessment of the power in band B relative to the overall frequency range, and hence, mitigating the impact of inter-subject variability. The potential variations captured by the ratio rP is illustrated in Figure 2 that depicts a varying spatial distribution pattern for each case (AD, FTD, HC), and band (alpha, delta, theta). A decrease in alpha and an increase in theta and delta power may be observed from HC to AD. These bands were chosen due to their known associations with cognitive functions and their reported dysregulation in dementia cases [47].

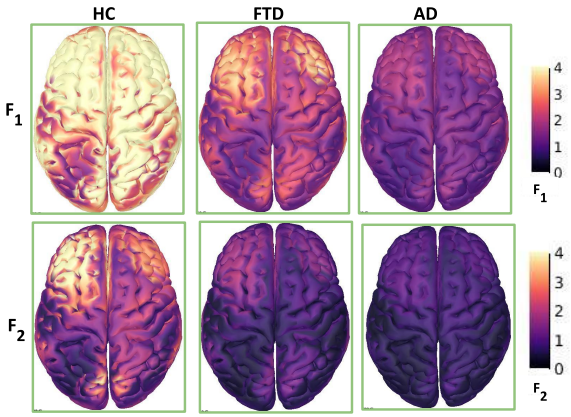

Fig. 3: Figure visually presents the different patterns across AD, FTD, and HC using F_1 and F_2. The Brainstorm toolbox is used to generate the plot.

2) Dementia Severity Index Computation: A decrease in alpha and an increase in theta and delta power for FTD and AD cases, are utilized in this Section to formulate the DSI. Subsequently, DSI will be employed for dementia classification. Following two specific feature sets are derived

utilizing Equation 4.

$$F_1 = \frac{rP_\alpha}{rP_\theta} \tag{5}$$

$$F_2 = \frac{rP_\alpha}{rP_\delta} \tag{6}$$

DSI is now constructed using the feature sets (F_1 and F_2) as follows:

$$DSI = \begin{cases} 0, & 0 < F_i \leq T_1 \\ 1, & T_1 < F_i \leq T_2 \\ 2, & F_i > T_2 \end{cases} \tag{7}$$

where, T_1 and T_2 are the thresholds that delineate severity levels detailed in Section III-B. The definition of DSI suggests that the lower values will correspond to potentially greater dementia severity. The dementia severity classification using DSI is additionally validated using machine learning algorithms applied to the derived feature sets F_i as detailed in Figure 4. The performance metrics and the associated procedure followed in classification, are detailed next.

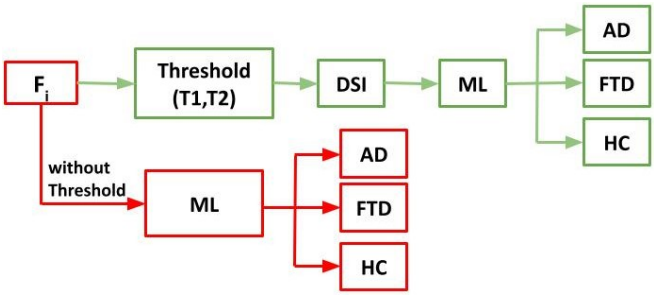

Fig. 4: Schematic diagram for classification of AD, FTD, and HC with and without thresholding approaches. Here, $DSI$and ML denote the dementia severity index and machine learning, respectively.

F. Classification

1) Performance Metrics: Random Forest (RF) and K-nearest neighbor (kNN) algorithms are employed to validate the effectiveness of the classification approach. Both the algorithms make use of a rigorous 10-fold cross-validation procedure, ensuring robust and generalizable results. The classification (distinguishing AD, FTD, and HC) performance is evaluated using the standard metrics (accuracy, sensitivity, and specificity), defined as

$$\text{Accuracy} = \frac{TN + TP}{TN + TP + FN + FP} \tag{8}$$

$$\text{Sensitivity} = \frac{TP}{TP + FN} \tag{9}$$

$$\text{Specificity} = \frac{TN}{TN + FP} \tag{10}$$

where TP, TN, FP, and FN correspond to True Positive, True Negative, False Positive, and False Negative, respectively.

2) Validating Feature Ability to Reflect Cognitive Performance: To further assess the feature capacity to capture individual variations in cognitive performance, a correlation with Mini-Mental State Examination (MMSE) score [48] is additionally investigated. The Spearman rank correlation coefficient (r) [49] is employed to quantify the relationship between actual MMSE scores and predicted MMSE values. The actual MMSE score is assessed through standard MMSE administration, while the predicted MMSE is derived from the computed features (F_1, F_2) using linear regression. The correlation analysis evaluates the effectiveness of the features in reflecting individual variations in cognitive performance. Initially, $\tilde{S}$, F_1 and F_2 features are examined to identify which feature shows the highest correlation. Subsequently, the effective feature correlation across all brain regions is indicated using $\tilde{S}_R$. High correlation coefficients would suggest a strong association between the features and actual MMSE scores, demonstrating the potential of these features as valuable tools for assessing cognitive decline in dementia patients.

To ensure robust and independent assessments, the Leave-One-Out cross-validation (LOOCV) method is adopted [50]. In this approach, the regression model is trained on data from all subjects except one, who serves as the "left-out" subject for prediction. This process is repeated iteratively, leaving out each subject once. Hence, this method provides a more reliable estimate of the model's generalizability.

3) Dimensionality Reduction in MMSE Prediction:: The proposed feature sets (F_1, F_2) capture spatial information from 15002 source (or vertices) points ($\tilde{S}$) and 68 regions ($\tilde{S}_R$) for each subject. This high dimensionality poses potential computational challenges for the linear regression model to predict MMSE scores. To overcome this, neighborhood component analysis (NCA) is implemented for dimensionality reduction.

NCA is a powerful machine learning technique that can effectively transform the high-dimensional data into a significantly lower-dimensional space $(e.g., twodimensions)$ [51]. In particular, NCA is utilized here to convert each $\tilde{S}$ and $\tilde{S}_R$ features into two dimensions. This reduction is achieved while critically preserving the key information relevant to MMSE prediction. The NCA implementation facilitates efficient and accurate MMSE prediction using the reduced-dimension features (F_1, F_2), highlighting their potential as a practical tool for assessing cognitive decline in dementia patients.

III. Experimental Conditions and Results

A. Experimental Conditions

The study utilizes preprocessed time series signals (V, $\tilde{S}$, and $\tilde{S}_R$) as inputs for computing relative band power (rP) in delta, theta, and alpha frequency bands, as detailed in SectionII-E.1. To comprehensively explore the effect of potential variations in rP across temporal scales, rP for various non-overlapping time window segments ranging from 2 to 40 seconds is computed. These rP values, obtained for each window segment across the entire time series signal and

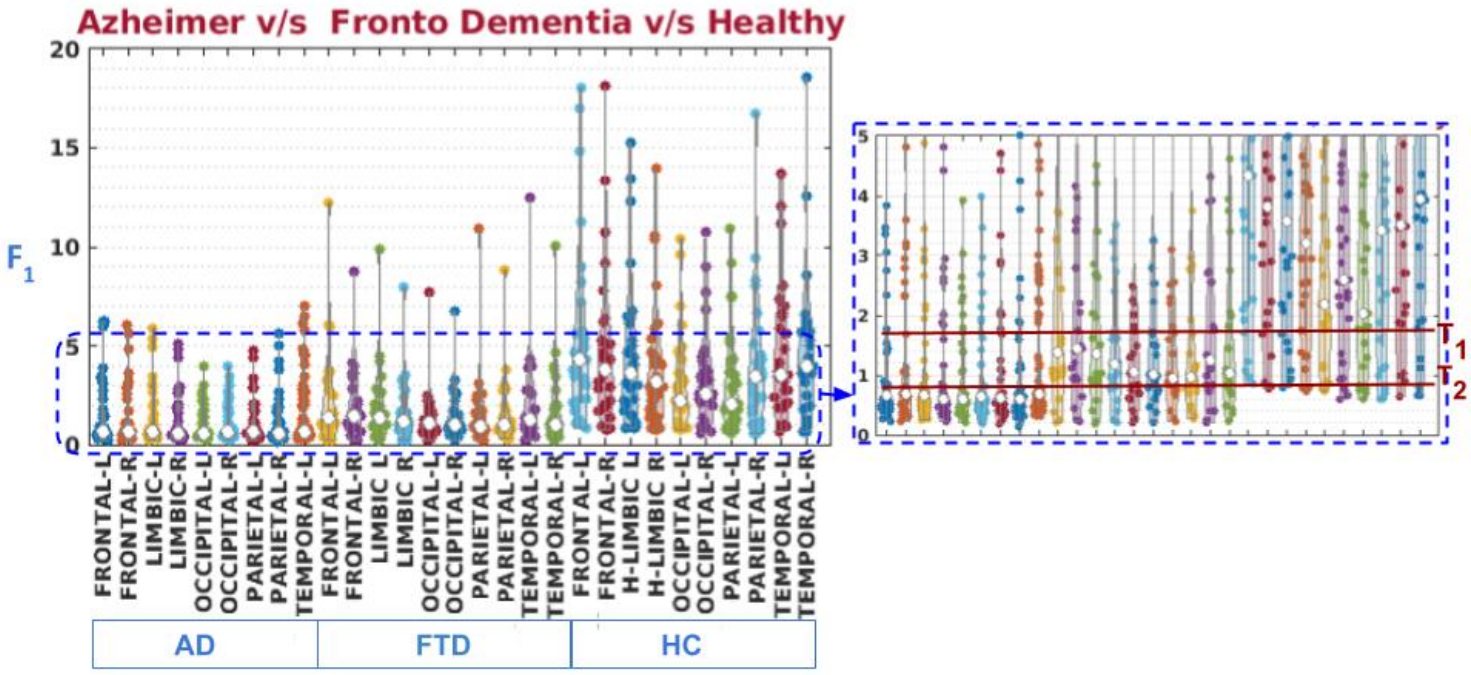

Fig. 5: This figure depicts the distribution of mean F_1 ratios for different brain lobes across subjects with AD, FTD, and HC. Each data point represents the mean F_1 value for a specific lobe in an individual subject. The violin plots show the probability density of these mean F_1 values for each lobe across all subjects within each group (AD, FTD, HC). T_1 and T_2 denote two chosen threshold levels. Wider sections of the violin plots, particularly around T_1 and T_2, indicate a higher probability of subjects within that group falling within the corresponding F_1 range for that specific lobe (i.e., higher probability for values near 0.9 and 2).

TABLE II: The table illustrates a comparison between the sensor and source domains, showcasing the superior performance of F_1 and F_2 computed from the source domain scout time series signals in contrast to the 19-channel time series signals in the sensor domain for the classification of AD, FTD, and HC.

Feature	Model	Accuracy (Source)	Accuracy (Sensor)
F_1	kNN	**87.88± 2.99**	67.54±1.84
	RF	**86.25±2.09**	65.66±1.61
F_2	kNN	**81.96±2.50**	66.782±2.16
	RF	**78.01±3.89**	66.141±3.17

TABLE III: Mean classification accuracy of RF classifier for classifying the AD, FTD, HC cases at different time windows.

Window (sec)	Classification
4	77.6
8	88.4
16	88.7
20	**89.2**
24	87.4
30	76.4
40	70.4

all subjects were utilized as features for classification into three classes: AD, FTD, and HC. RF algorithm was utilized for this. To identify the optimal temporal representation for subsequent analysis, a data-driven approach was employed. In particular, classification accuracy was evaluated for each window segment, taking $\tilde{S_R}$ as input. The accuracy is presented in Table III. It may be noted that the 20-second window yields the highest classification accuracy of 89.2%. Hence, a window segment of 20 seconds was utilized for computing rP for further analysis. This approach ensured that the chosen window size captures the most informative temporal dynamics of the rP features for characterizing group differences. For each frame, F_1 and F_2 and their corresponding DSI values were computed from rP. It is to note that for a given EEG data of length $L(= 240s)$ from $N_s(= 88)$ subjects, selected window segment $W(= 20s)$ and, chosen parameter $K(= 19$ for $V, 68$ for $\tilde{S}_R)$, the feature matrix comprises of $\frac{L \times N_s}{W} \times K$ dimensions.

The efficacy of the proposed framework is rigorously validated by implementing a user-dependent, 10-fold cross-validation strategy. For each fold, 80% of the subjects' data served for training the machine learning models, while the remaining 20% were used for testing. The accuracies, sensitivities, and specificities obtained from each fold were then averaged to provide a robust estimate the generalizability of the models. This rigorous validation was performed

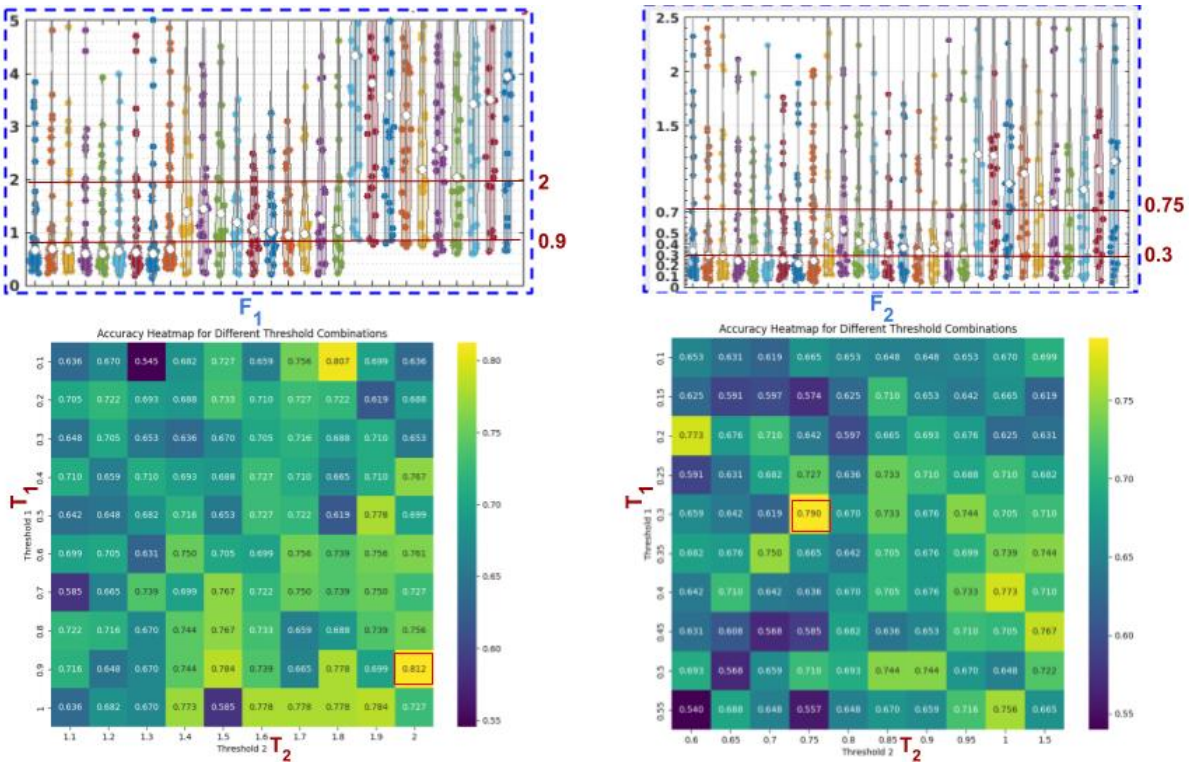

Fig. 6: The figure illustrates the T_1 and T_2 values for both F_1 and F_2, which are employed to calculate their respective DSI. The accompanying heatmap below showcases the accuracy values corresponding to various threshold combinations. Notably, the red blocks highlight the optimal T_1 and T_2 combinations in both F_1 and F_2 for computing the DSI.

to evaluate the effectiveness of the chosen features and the potential merit of the DSI thresholding approach for stratifying dementia severity levels. The training parameters employed for the machine learning models were the default parameters of the sklearn library. The statistical significance of the features and derived DSI values across different cases was assessed using the paired t-test method.

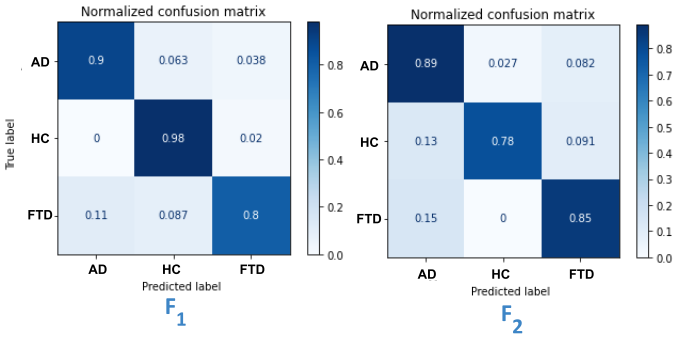

Fig. 7: The figure compares the classification performance of F_1 (left) and F_2 (right) features by presenting confusion matrices for each. Columns represent predicted groups, while rows represent actual groups. Diagonal cells indicate correctly classified subjects, while off-diagonal cells represent misclassifications.

B. Results

It may be noted from Figure 3 that there is a clear distinction in the spatial distribution of individuals with AD, FTD, and HC when using the proposed features F_1 and F_2 with input $\tilde{S}$. A comparison between sensor (V) and source domains ($\tilde{S}_R$ is presented in Table II. Figure 5 illustrates the probability distributions of mean F_1 for all cases (AD, FTD, and HC) and subjects. The wider section of the plot represents the likelihood of each case exhibiting this mean F_1 which influences the threshold T_1 and T_2. Specifically, the minimum of all means or likelihood for the F and H cases is utilized as T_1 and T_2 respectively. The threshold values are further utilized to compute the DSI. The DSI values $\{0, 1, 2\}$ corresponds to $\{$AD, FTD, HC $\}$ respectively. Figure 6 explores different threshold combinations to indicate the efficacy. It is noted that the best accuracy for $\{T_1, T_2\}$ is achieved at $\{0.9, 2\}$ for F_1 and at $\{0.3, 0.75\}$ for F_2.

The efficacy of DSI in classifying different dementia cases and healthy controls is further explored using machine learning algorithms (kNN and RF). The mean classification accuracy, sensitivity, and specificity for 10-fold cross-validation are presented in Table IV. The corresponding confusion matrix using $\{F_1, F_2\}$ is presented in Figure 7 and using $\{DSI_{F_1}, DSI_{F_2}\}$ in Figure 8. Additionally, the effectiveness of the threshold-based approach, DSI, is examined on another dataset, as detailed in Table V.

Motivated by the high accuracy (87.88% for F_1, as pre-

TABLE IV: Table compares the performance of F_1 and F_2 features, along with their corresponding DSI values, in classifying subjects with AD, HC, and FTD using various machine learning algorithms (kNN, RF) and 10-fold cross-validation. The kNN model achieved higher accuracy with F_1 features (87.88%) compared to F_2 features (81.96%). This suggests F_1 may be a more informative feature for distinguishing dementia groups. DSI values derived from F_1 features also yielded better classification accuracy (81.62%) compared to DSI from F_2 features (73.12%) using the kNN model. This indicates that DSI based on F_1 values potentially retains valuable information for dementia severity stratification.

	Machine Learning Model	**Accuracy**	**Specificity**	**Sensitivity**
		Mean±Standard Deviation	**Mean ± Standard Deviation**	**Mean±Standard Deviation**
DSI_{F1}	kNN	**81.62± 1.36**	89.34± 1.19	80.47±1.61
	RF	81.37±2.13	89.83±1.95	81.31±3.28
F_1	kNN	**87.88± 2.99**	93.17±1.85	87.21±2.86
	RF	86.25±2.09	92.58±1.30	85.97±2.34
DSI_{F2}	kNN	73.12±1.82	84.07±1.21	72.89±4.00
	RF	72.46±3.67	83.80±2.46	71.78±3.83
F_2	kNN	81.96±2.50	89.84±1.56	81.17±2.60
	RF	78.01±3.89	87.51±2,42	76.84±4.21

sented in Table IV), potential clinical relevance is further explored by computing correlation with Mini-Mental State Examination (MMSE) score. In particular, the correlation between the predicted MMSE score obtained using F_1 and F_2 and the actual MMSE of all subjects is computed. The correlation values provide insights into cognitive impairment, as depicted in Figure 9. It is to note that F_1 provides a higher correlation with MMSE.

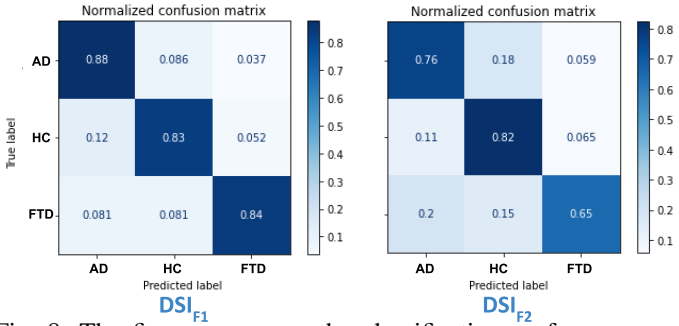

Fig. 8: The figure compares the classification performance of DSI derived from F_1 (left) and F_2 (right) features by presenting confusion matrices for each. Columns represent predicted groups, while rows represent actual groups. Diagonal cells indicate correctly classified subjects, while off-diagonal cells represent misclassifications. Analyzing the distribution of these values can reveal potential strengths and weaknesses of each feature-based DSI for dementia classification.

TABLE V: This table illustrates the classification performance of F_1 features and their corresponding DSI values across distinct datasets. The analysis incorporates diverse machine learning algorithms (kNN, RF) and employs 10-fold cross-validation to differentiate between subjects with AD and HC

Dataset2

Model	**Accuracy**		**Specificity**		**Sensitivity**	
	DSI_{F1}	F_1	DSI_{F1}	F_1	DSI_{F1}	F_1
kNN	90.9	95.45	89.28	92.85	87.71	92.27
RF	90.9	100	100	100	100	100

C. Discussion

1) F_1 and F_2 Analysis: : This section evaluates the efficacy of the proposed classification of dementia cases and identifies the most effective features. The F_1 ($p < 0.05$) and F_2 ($p < 0.05$) features of the processed scalp potential V and the source-domain scout time series ($\tilde{S}_R$), were utilized as inputs for the machine learning models that include RF and kNN. It may be noted from Table II that higher classification accuracy is achieved when utilizing the source-domain scout time series. Hence, the source domain approach is further analyzed. A comparison between F_1 and F_2 is presented in Table IV and Figure 7. It may be noted that the highest classification accuracy of 87.88% is achieved when the F_1 feature is utilized. In particular, positive AD, FTD, and HC cases are correctly identified with approximately 6% and 9% higher accuracy in kNN and RF classification models respectively, when the F_1 feature is considered. For actual negative cases also, the F_1 feature outperforms F_2 with a difference of approximately 3% in kNN and 5% in RF. The previous studies have associated a slowing of the EEG with both F and A [54], [55], [56]. Both the proposed features F_1 and F_2, capture the slowing parameter. However, the distinctive F_1 feature demonstrates superior effectiveness in capturing the differentiation, resulting in the highest accuracy. The findings are further validated by Figure 3, which illustrates clear distinctions among AD, FTD, and HC cases when the F_1 feature is utilized. Notably, the highest value of F_1 is predominantly observed in HC, a comparatively lower value in FTD, and the lowest in AD cases. This reinforces the discriminatory power of F_1 in capturing the underlying patterns.

2) Dementia Severity Index: : In this Section, F_1 and F_2 features from scout time series information, are analyzed for each subject to derive DSI values through the threshold approach outlined in Equation 7. The resulting threshold values T_1 and T_2 are determined based on the likelihood of each case (AD, FTD, HC) as illustrated in Figure 5 and Figure 6. To assess the effectiveness of the proposed threshold-based approach in classifying dementia cases (AD, FTD) alongside HC, the corresponding DSIs of F_1 ($p < 0.05$) and

TABLE VI: Comparative Analysis of Various Methods for AD, FTD, and HC classification.

Authors	Sample (A/F/CN)	Methodology	Classification Problem	Results		
				Accuracy	Sensitivity	Specificity
Fiscon D. et al [23]	86-0-23	Discrete Fourier transform, wavelet analysis, decision trees	A/CN	83	-	-
Caso et al. [24]	39-39-39	Relative power of EEG rhythms, sLORETTA, ANOVA analysis	A + F/CN	-	44.87	85
			A/F	-	48.72	85
Dottori et al. [52]	13-13-25	Connectivity features, SVM	A and F/CN	54	-	-
			A/F	73	-	-
			A/CN	73	-	-
Nishida et al. [25]	19-19-22	EEG rhythms energy, sLORETTA, kNN	F/CN	85.80	55.00	84.00
			A/CN	92.80	74.00	73.00
			F/A	89.80	74.00	63.00
Miltiadous, Andreas, et al. [53]	10-10-8	Energy, mean, variance, IQR, random forests, decision trees	A/CN	78.5	82.4	74
			F/CN	86.3	87	83
Proposed Method	**36-23-29**	DSI_{F1}	**AD/FTD/HC**	**81.627±1.36**	**80.476±1.61**	**89.348±1.19**
		F_1	**AD/FTD/HC**	**87.889±2.99**	**87.212±2.86**	**93.178±1.85**

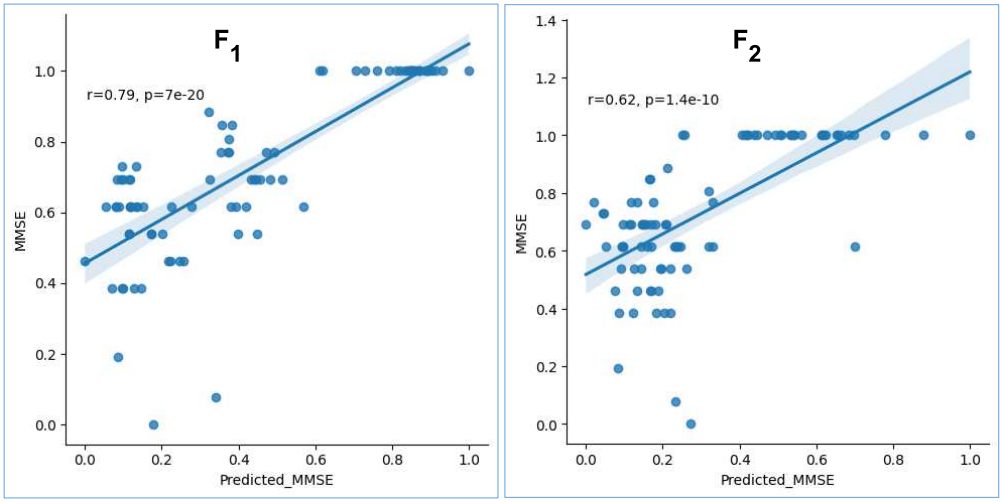

Fig. 9: The figure illustrates the correlation between the predicted MMSE using features F_1 (on the left) and F_2 (on the right). These features were extracted from the time series signals of source vertices and then dimensionality reduced to 2 using NCA. Notably, F_1 exhibited a stronger relationship with MMSE, as indicated by the higher Spearman Correlation coefficient (r = 0.79), suggesting its potential for enabling non-invasive assessment of cognitive decline.

F_2 ($p < 0.05$) are employed as inputs to the kNN and RF models. The results in Table IV and Figure 8 reveal that the highest classification accuracy of 81.62% is achieved when DSI_{F1} is considered. The model demonstrates superior performance in accurately identifying positive cases of AD, FTD, and HC using DSI_{F1}, with approximately 7% and 9% higher accuracy in kNN and RF, respectively. Similarly, when considering actual negative cases, DSI_{F1} outperforms DSI_{F2} with a difference of approximately 5% in kNN and 6% in RF. This suggests that DSI based on the F_1 feature, retains valuable information for stratifying dementia severity. To evaluate the reliability of the proposed threshold-based approach, DSI_{F1} was computed on an additional dataset [57] involving only two groups of AD and HC cases. The results in Table V affirm the potential of the threshold-based approach in dementia classification. A comparative analysis of various methods and classification problems is presented in Table VI. It may be noted that in the category of three class classification problem case, the propose approach provides the highest accuracy. The threshold values T_1 = 0.9 and T_2 = 2 were utilized. These values provide insight into identifying the range and assign quantitative values to different dementia conditions during rest. This approach also contributes to reducing computation time by eliminating the need to train a machine learning model for classifying dementia and healthy individuals.

3) Cognitive Performance Analysis:: This investigation delves into the relationship between the proposed features $\{F_1, F_2\}$ and the Mini-Mental State Examination (MMSE) score with the aim of exploring their potential as a non-invasive means to assess cognitive decline. The MMSE serves as a comprehensive short screening tool for measuring cognitive impairment in various settings, including clinical, research, and community contexts [58]. To predict MMSE, the study adopted a LOOCV approach, employing linear regression and the NCA model for the source domain ($\tilde{S_R}$) F_1 and F_2 features. Figure 9 illustrates the Spearman correlation coefficients (r) between the predicted MMSE using F_1 and F_2 and the actual MMSE. The F_1 feature demonstrated a higher correlation value when compared to F_2. A higher correlation signifies a more robust alignment between the model's predictions and the actual cognitive function. Brain regions with higher correlations are promising candidates as a potential biomarker for cognitive impairment, as indicated

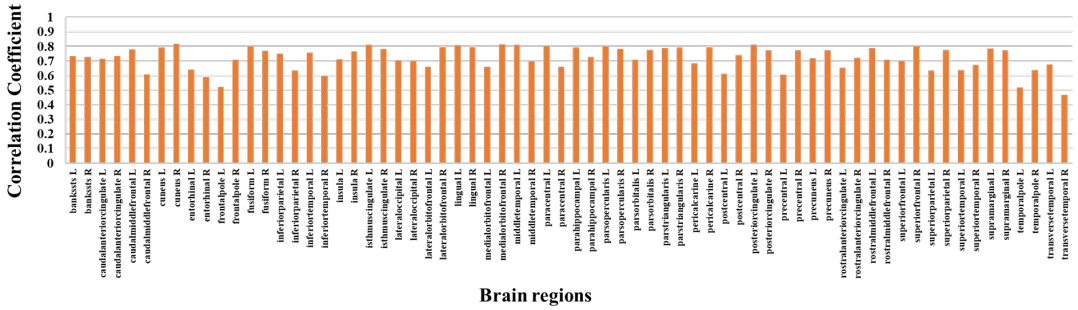

Fig. 10: This figure illustrates the Spearman correlation coefficients (r) between predicted Mini-Mental State Examination (MMSE) scores and actual MMSE scores across 68 brain regions. The predictions were generated using a linear regression model with F_1 features. Higher correlation values in specific regions signify a stronger relationship between F_1-based MMSE predictions and actual cognitive function in those areas. Here,'R' and 'L' denote the right and left brain regions, respectively.

by the distinctive features captured by F_1 in Figure 10.

IV. Conclusion

The study presents an efficient method to classify AD, FTD, and HC from resting state EEG. In particular, two features F_1 and F_2 are presented as potential biomarkers for cognitive decline. The examination of F_1 and F_2 features reveal that F_1 as a distinct feature, significantly elevates the accuracy of dementia classification. The evident distinctions among AD, FTD, and HC based on F_1 values highlight its discriminatory power. The introduction of the Dementia Severity Index (DSI) a threshold-based approach based on F_1 and F_2, further fortifies the methodology. The achieved high classification accuracy (81.62%) and the superior performance of DSI_{F1} in identifying positive cases highlight the potential of this approach in stratifying dementia severity. Additionally, the assignment of quantitative values to different dementia conditions during rest enhances the interpretability of the findings. Validation on two diverse EEG datasets adds robustness to DSI, reinforcing the practical utility of the proposed threshold-based method. The exploration into cognitive performance, specifically the relationship between F_1 features and the commonly used Mini-Mental State Examination (MMSE), presents a promising objective avenue for non-invasive cognitive decline assessment. The correlation analysis identifies brain regions with higher correlations as potential biomarkers for cognitive impairment. Moreover, the proposed threshold-based approach not only improves classification accuracy but also offers a practical advantage by reducing extensive subjective assessment. In essence, the study makes a meaningful contribution to the field of dementia research, providing valuable tools and insights for both classifying and assessing dementia cases. The effective features identified along with the proposed methodology, hold promise for advancing our understanding and diagnosis of dementia-related conditions.

Acknowledgment

The authors extend their thanks to Ayush Tripathi for his valuable insights during manuscript drafting and the Multichannel Signal Processing Laboratory (MSP Lab) at the Indian Institute of Technology Delhi (IIT Delhi).

Authors' contributions

L.K. supervised the entire project; S.R. designed the study. Data analysis by S.R.; interpretation of results by S.R. and L.K.; writing and figure preparation of the original draft by S.R.; writing & editing by S.R. and L.K. All authors critically reviewed the manuscript.

Funding

This research work was supported in part by IIT Mandi iHub and HCI Foundation India with project number RP04502G.

Availability of data and materials

The datasets generated and/or analyzed in the present study are available from the corresponding author upon reasonable request.

Declarations

Ethics approval and consent to participate

Not applicable. This study utilized publicly available EEG datasets.

Consent for publication

Not applicable.

Competing interests

The authors declare no competing interests.

References

[1] H. Chertkow, H. H. Feldman, C. Jacova, F. Massoud, Definitions of dementia and predementia states in alzheimer's disease and vascular cognitive impairment: consensus from the canadian conference on diagnosis of dementia, Alzheimer's research & therapy 5 (1) (2013) 1–8.

[2] P. dos Santos, C. Leide, P. F. Ozela, M. de Fatima de Brito Brito, A. A. Pinheiro, E. C. Padilha, F. S. Braga, d. S. de Paula, H. Carlos, C. B. R. dos Santos, et al., Alzheimer's disease: a review from the pathophysiology to diagnosis, new perspectives for pharmacological treatment, Current medicinal chemistry 25 (26) (2018) 3141–3159.

[3] M. A. Maito, H. Santamaría-García, S. Moguilner, K. L. Possin, M. E. Godoy, J. A. Avila-Funes, M. I. Behrens, I. L. Brusco, M. A. Bruno, J. F. Cardona, et al., Classification of alzheimer's disease and frontotemporal dementia using routine clinical and cognitive measures across multicentric underrepresented samples: A cross sectional observational study, The Lancet Regional Health–Americas 17 (2023).

[4] M. Prince, R. Bryce, E. Albanese, A. Wimo, W. Ribeiro, C. P. Ferri, The global prevalence of dementia: a systematic review and metaanalysis, Alzheimer's & dementia 9 (1) (2013) 63–75.

[5] A. Wimo, B. Winblad, H. Aguero-Torres, E. von Strauss, The magnitude of dementia occurrence in the world, Alzheimer Disease & Associated Disorders 17 (2) (2003) 63–67.

[6] M. Weytingh, P. Bossuyt, H. Van Crevel, Reversible dementia: more than 10% or less than 1%? a quantitative review, Journal of neurology 242 (1995) 466–471.

[7] W. Jaroudi, J. Garami, S. Garrido, M. Hornberger, S. Keri, A. A. Moustafa, Factors underlying cognitive decline in old age and alzheimer's disease: the role of the hippocampus, Reviews in the Neurosciences 28 (7) (2017) 705–714.

[8] A. Geraudie, P. Battista, A. M. García, I. E. Allen, Z. A. Miller, M. L. Gorno-Tempini, M. Montembeault, Speech and language impairments in behavioral variant frontotemporal dementia: a systematic review, Neuroscience & Biobehavioral Reviews 131 (2021) 1076–1095.

[9] L. Chouliaras, J. T. O'Brien, The use of neuroimaging techniques in the early and differential diagnosis of dementia, Molecular Psychiatry (2023) 1–14.

[10] J. C. Morris, The clinical dementia rating (cdr) current version and scoring rules, Neurology 43 (11) (1993) 2412–2412.

[11] M. F. Folstein, S. E. Folstein, P. R. McHugh, "mini-mental state": a practical method for grading the cognitive state of patients for the clinician, Journal of psychiatric research 12 (3) (1975) 189–198.

[12] Z. S. Nasreddine, N. A. Phillips, V. Bédirian, S. Charbonneau, V. Whitehead, I. Collin, J. L. Cummings, H. Chertkow, The montreal cognitive assessment, moca: a brief screening tool for mild cognitive impairment, Journal of the American Geriatrics Society 53 (4) (2005) 695–699.

[13] D. Bruno, S. Schurmann Vignaga, Addenbrooke's cognitive examination iii in the diagnosis of dementia: a critical review, Neuropsychiatric disease and treatment (2019) 441–447.

[14] M. Mendez, Chapter 16—general mental status scales, rating instruments, and behavior inventories, The mental status examination handbook. Philadelphia: Elsevier (2022) 181–199.

[15] J. W. Kim, D. Y. Lee, E. H. Seo, B. K. Sohn, Y. M. Choe, S. G. Kim, S. Y. Park, I. H. Choo, J. C. Youn, J. H. Jhoo, et al., Improvement of screening accuracy of mini-mental state examination for mild cognitive impairment and non-alzheimer's disease dementia by supplementation of verbal fluency performance, Psychiatry Investigation 11 (1) (2014) 44.

[16] Q. Yu, Y. Mai, Y. Ruan, Y. Luo, L. Zhao, W. Fang, Z. Cao, Y. Li, W. Liao, S. Xiao, et al., An MRI-based strategy for differentiation of frontotemporal dementia and alzheimer's disease, Alzheimer's research & therapy 13 (2021) 1–12.

[17] S. Suri, A. Topiwala, C. E. Mackay, K. P. Ebmeier, N. Filippini, Using structural and diffusion magnetic resonance imaging to differentiate the dementias, Current neurology and neuroscience reports 14 (2014) 1–14.

[18] J. Akhila, C. Markose, R. Aneesh, Feature extraction and classification of dementia with neural network, in: 2017 International Conference on Intelligent Computing, Instrumentation and Control Technologies (ICICICT), IEEE, 2017, pp. 1446–1450.

[19] L. H. Meeter, L. D. Kaat, J. D. Rohrer, J. C. Van Swieten, Imaging and fluid biomarkers in frontotemporal dementia, Nature Reviews Neurology 13 (7) (2017) 406–419.

[20] M. Cejnek, O. Vysata, M. Valis, I. Bukovsky, Novelty detection-based approach for alzheimer's disease and mild cognitive impairment diagnosis from EEG, Medical & Biological Engineering & Computing 59 (2021) 2287–2296.

[21] L.-M. Sánchez-Reyes, J. Rodríguez-Reséndiz, G. N. Avecilla-Ramírez, M.-L. García-Gomar, J.-B. Robles-Ocampo, Impact of EEG parameters detecting dementia diseases: A systematic review, IEEE Access 9 (2021) 78060–78074.

[22] M. Lindau, V. Jelic, S.-E. Johansson, C. Andersen, L.-O. Wahlund, O. Almkvist, Quantitative eeg abnormalities and cognitive dysfunctions in frontotemporal dementia and alzheimer's disease, Dementia and geriatric cognitive disorders 15 (2) (2003) 106–114.

[23] G. Fiscon, E. Weitschek, A. Cialini, G. Felici, P. Bertolazzi, S. De Salvo, A. Bramanti, P. Bramanti, M. C. De Cola, Combining eeg signal processing with supervised methods for alzheimer's patients classification, BMC medical informatics and decision making 18 (1) (2018) 1–10.

[24] F. Caso, M. Cursi, G. Magnani, G. Fanelli, M. Falautano, G. Comi, L. Leocani, F. Minicucci, Quantitative EEG and LORETA: valuable tools in discerning ftd from ad?, Neurobiology of aging 33 (10) (2012) 2343–2356.

[25] K. Nishida, M. Yoshimura, T. Isotani, T. Yoshida, Y. Kitaura, A. Saito, H. Mii, M. Kato, Y. Takekita, A. Suwa, et al., Differences in quantitative EEG between frontotemporal dementia and alzheimer's disease as revealed by loreta, Clinical Neurophysiology 122 (9) (2011) 1718–1725.

[26] A. Miltiadous, K. D. Tzimourta, T. Afrantou, P. Ioannidis, N. Grigoriadis, D. G. Tsalikakis, P. Angelidis, M. G. Tsipouras, E. Glavas, N. Giannakeas, A. T. Tzallas, "a dataset of EEG recordings from: Alzheimer's disease, frontotemporal dementia and healthy subjects" (2023). doi:doi:10.18112/openneuro.ds004504.v1.0.6.

[27] I. Math Works, Matlab. version 2020a (2020).

[28] A. Delorme, S. Makeig, EEGLAB: an open source toolbox for analysis of single-trial EEG dynamics including independent component analysis, Journal of neuroscience methods 134 (1) (2004) 9–21.

[29] C.-Y. Chang, S.-H. Hsu, L. Pion-Tonachini, T.-P. Jung, Evaluation of artifact subspace reconstruction for automatic artifact components removal in multi-channel EEG recordings, IEEE Transactions on Biomedical Engineering 67 (4) (2019) 1114–1121.

[30] T.-P. Jung, S. Makeig, C. Humphries, T.-W. Lee, M. J. Mckeown, V. Iragui, T. J. Sejnowski, Removing electroencephalographic artifacts by blind source separation, Psychophysiology 37 (2) (2000) 163–178.

[31] C. Babiloni, D. Jakhar, F. Tucci, C. Del Percio, S. Lopez, A. Soricelli, M. Salvatore, R. Ferri, V. Catania, F. Massa, et al., Resting state electroencephalographic alpha rhythms are sensitive to alzheimer's disease mild cognitive impairment progression at a 6-month follow-up, Neurobiology of Aging (2024).

[32] A. Zaitcev, EEG source imaging for improved control bci performance, Ph.D. thesis, University of Sheffield (2017).

[33] C. M. Michel, D. Brunet, "EEG source imaging: a practical review of the analysis steps", Frontiers in neurology 10 (2019) 325. doi:https://doi.org/10.3389/fneur.2019.00325.

[34] H. Hallez, B. Vanrumste, R. Grech, J. Muscat, W. De Clercq, A. Vergult, Y. D'Asseler, K. P. Camilleri, S. G. Fabri, S. Van Huffel, et al., Review on solving the forward problem in EEG source analysis, Journal of neuroengineering and rehabilitation 4 (1) (2007) 1–29.

[35] S. Baillet, J. Riera, G. Marin, J. Mangin, J. Aubert, L. Garnero, "Evaluation of inverse methods and head models for EEG source localization using a human skull phantom", Physics in medicine & biology 46 (1) (2001) 77. doi:https://doi.org/10.1088/0031-9155/46/1/306.

[36] G. Niso, F. Tadel, E. Bock, M. Cousineau, A. Santos, S. Baillet, Brainstorm pipeline analysis of resting-state data from the open meg archive, Frontiers in neuroscience 13 (2019) 284.

[37] C. Qin, R. Yang, M. Huang, W. Liu, Z. Wang, Spatial variation generation algorithm for motor imagery data augmentation: Increasing the density of sample vicinity, IEEE Transactions on Neural Systems and Rehabilitation Engineering (2023).

[38] A. G. Baroumand, A. A. Arbune, G. Strobbe, V. Keereman, L. H. Pinborg, M. Fabricius, G. Rubboli, C. G. Madsen, B. Jespersen, J. Brennum, et al., Automated ictal EEG source imaging: A retrospective, blinded clinical validation study, Clinical Neurophysiology 141 (2022) 119–125.

[39] F. Sperli, L. Spinelli, M. Seeck, M. Kurian, C. M. Michel, G. Lantz, EEG source imaging in pediatric epilepsy surgery: a new perspective in presurgical workup, Epilepsia 47 (6) (2006) 981–990.

[40] R. D. Pascual-Marqui, et al., Standardized low-resolution brain electromagnetic tomography (sloreta): technical details, Methods Find Exp Clin Pharmacol 24 (Suppl D) (2002) 5–12.

[41] R. D. Pascual-Marqui, D. Lehmann, T. Koenig, K. Kochi, M. C. Merlo, D. Hell, M. Koukkou, "Low resolution brain electromagnetic tomography (LORETA) functional imaging in acute, neuroleptic-naive, first-episode, productive schizophrenia", Psychiatry Research: Neuroimaging 90 (3) (1999) 169–179. doi:https://doi.org/10.1016/s0925-4927(99)00013-x.

[42] M. A. Jatoi, N. Kamel, A. S. Malik, I. Faye, "EEG based brain source localization comparison of sLORETA and eLORETA", Australasian physical & engineering sciences in medicine 37 (2014) 713–721. doi:https://doi.org/10.1007/s13246-014-0308-3.

[43] R. S. Desikan, F. Ségonne, B. Fischl, B. T. Quinn, B. C. Dickerson, D. Blacker, R. L. Buckner, A. M. Dale, R. P. Maguire, B. T. Hyman, M. S. Albert, R. J. Killiany, An automated labeling system for subdividing the human cerebral cortex on MRI scans into gyral based regions of interest, NeuroImage 31 (3) (2006) 968–980. doi:https://doi.org/10.1016/j.neuroimage.2006.01.021.

[44] A. Giustiniani, L. Danesin, B. Bozzetto, A. Macina, S. Benavides-Varela, F. Burgio, Functional changes in brain oscillations in dementia: A review, Reviews in the Neurosciences 34 (1) (2023) 25–47.

[45] E. Başar, B. Güntekin, Review of delta, theta, alpha, beta, and gamma response oscillations in neuropsychiatric disorders, Supplements to Clinical neurophysiology 62 (2013) 303–341.

[46] F. Tadel, E. Bock, G. Niso, J. C. Mosher, M. Cousineau, D. Pantazis, R. M. Leahy, S. Baillet, "MEG/EEG group analysis with brainstorm", Frontiers in neuroscience (2019) 76doi:https://doi.org/10.3389/fnins.2019.00076.

[47] J. Jeong, Eeg dynamics in patients with alzheimer's disease, Clinical neurophysiology 115 (7) (2004) 1490–1505.

[48] M. S. Mega, J. L. Cummings, T. Fiorello, J. Gornbein, The spectrum of behavioral changes in alzheimer's disease, Neurology 46 (1) (1996) 130–135.

[49] G. I. Allen, N. Amoroso, C. Anghel, V. Balagurusamy, C. J. Bare, D. Beaton, R. Bellotti, D. A. Bennett, K. L. Boehme, P. C. Boutros, et al., Crowdsourced estimation of cognitive decline and resilience in alzheimer's disease, Alzheimer's & Dementia 12 (6) (2016) 645–653.

[50] M. Bucholc, X. Ding, H. Wang, D. H. Glass, H. Wang, G. Prasad, L. P. Maguire, A. J. Bjourson, P. L. McClean, S. Todd, et al., A practical computerized decision support system for predicting the severity of alzheimer's disease of an individual, Expert systems with applications 130 (2019) 157–171.

[51] J. Goldberger, G. E. Hinton, S. Roweis, R. R. Salakhutdinov, Neighbourhood components analysis, Advances in neural information processing systems 17 (2004).

[52] M. Dottori, L. Sedeño, M. Martorell Caro, F. Alifano, E. Hesse, E. Mikulan, A. M. García, A. Ruiz-Tagle, P. Lillo, A. Slachevsky, et al., Towards affordable biomarkers of frontotemporal dementia: a classification study via network's information sharing, Scientific reports 7 (1) (2017) 3822.

[53] A. Miltiadous, K. D. Tzimourta, N. Giannakeas, M. G. Tsipouras, T. Afrantou, P. Ioannidis, A. T. Tzallas, Alzheimer's disease and frontotemporal dementia: A robust classification method of eeg signals and a comparison of validation methods, Diagnostics 11 (8) (2021) 1437.

[54] W. Klimesch, EEG alpha and theta oscillations reflect cognitive and memory performance: a review and analysis, Brain research reviews 29 (2-3) (1999) 169–195.

[55] C. S. Musaeus, K. Engedal, P. Høgh, V. Jelic, M. Mørup, M. Naik, A.-R. Oeksengaard, J. Snaedal, L.-O. Wahlund, G. Waldemar, et al., EEG theta power is an early marker of cognitive decline in dementia due to alzheimer's disease, Journal of Alzheimer's Disease 64 (4) (2018) 1359–1371.

[56] R. Kalluri, V. S. LeBleu, The biology, function, and biomedical applications of exosomes, Science 367 (6478) (2020) eaau6977.

[57] A. M. Pineda, F. M. Ramos, L. E. Betting, A. S. Campanharo, Quantile graphs for EEG-based diagnosis of Alzheimer's disease, Plos one 15 (6) (2020) e0231169. doi:https://doi.org/10.1016/j.jalz.2019.01.010.

[58] I. Arevalo-Rodriguez, N. Smailagic, M. R. i Figuls, A. Ciapponi, E. Sanchez-Perez, A. Giannakou, O. L. Pedraza, X. B. Cosp, S. Cullum, Mini-mental state examination (mmse) for the detection of alzheimer's disease and other dementias in people with mild cognitive impairment (mci), Cochrane Database of Systematic Reviews (3) (2015).